612 *Chem. Mater.* **2010,** *22,* 612–623
DOI:10.1021/cm901917a

CHEMISTRY OF MATERIALS
Review

Solid Solution of GaN and ZnO as a Stable Photocatalyst for Overall Water Splitting under Visible Light†

Kazuhiko Maeda and Kazunari Domen*

Department of Chemical System Engineering, The University of Tokyo, 7-3-1 Hongo, Bunkyo-ku, Tokyo 113-8656, Japan

Received June 30, 2009. Revised Manuscript Received August 18, 2009

Large-scale hydrogen production from water using only solar energy is an ultimate goal for the supply of clean, recyclable energy, and several reactions and schemes have been proposed. Overall water splitting using a particulate photocatalyst is one attractive solution with a wide range of applications. A number of photocatalysts have been proposed, and some have achieved high quantum efficiencies. Unfortunately, most of these photocatalysts consist of metal oxides and work only in the ultraviolet (UV) region. To effectively utilize solar energy, it is necessary to develop a material that will function under visible light. This paper reviews the recent development of such a photocatalyst, specifically focusing on efforts by the authors' group to prepare a solid solution of GaN and ZnO. This new material is capable of splitting water into hydrogen and oxygen under visible light ($\lambda > 400$ nm) with good reproducibility.

1. Introduction

Catalytic splitting of pure water into hydrogen and oxygen in the presence of semiconductor powders using visible light is a promising approach for storing solar energy as chemical energy.[1,2] The reaction (eq 1) is a typical "uphill reaction", having a large positive change in the Gibbs free energy ($\Delta G^0 = 238$ kJ/mol).

$$2H_2O \rightarrow 2H_2 + O_2 \quad (1)$$

The half-reactions are described as follows:

$$2H^+ + 2e^- \rightarrow H_2 \quad (2)$$

$$2H_2O + 4h^+ \rightarrow O_2 + 4H^+ \quad (3)$$

Research in this field was initially triggered by the demonstration of photoelectrochemical water splitting using a single-crystal titanium dioxide (rutile) photoanode and a platinum cathode with an external bias.[1] Over the past decades, while many semiconducting materials have been reported to be active for the reaction, none have demonstrated stable, reproducible overall water splitting capability under visible light irradiation. The major obstacle to progress in this field has been the lack of a suitable compound that meets the following three requirements: (1) a band gap narrower than 3 eV, (2) band-edge potentials suitable for overall water splitting, and (3) stability in the photocatalytic reaction. Specifically, the band gap must be sufficiently small to allow the absorption of visible light (< 3 eV), and the band edges must be located in a position that allows for the reduction and oxidation of water by photoexcited electrons and holes. In general, efficient photocatalytic materials contain either transition-metal cations with a d^0 electronic configuration (e.g., Ti^{4+} and Ta^{5+})[3−5] or typical metal cations with a d^{10} electronic configuration (e.g., In^{3+} and Sn^{4+})[6,7] as principal cation components.[8] The empty d or sp orbitals form the bottom of the conduction band. The top of the valence band of a metal-oxide photocatalyst with d^0- or d^{10}-metal cations usually consists of O2p orbitals, which are located at about $+3$ eV or higher vs a normal hydrogen electrode (NHE), thus producing a band gap too wide to absorb visible light.[9] As some nonoxide compounds such as CdS and CdSe have band edge potentials suitable for water splitting under visible light, these compounds were carefully examined for visible light utilization. However, no successful photocatalytic systems have been established because of a lack of oxygen production due to the instability of the materials.[10]

Because N2p orbitals have higher potential energy than O2p orbitals, it would be interesting to use a metal nitride or metal oxynitride as a photocatalyst. The authors' group has developed (oxy)nitrides, such as TaON,[11−14] Ta_3N_5,[15,16] and $LaTiO_2N$,[17,18] as potential candidates for overall water splitting under visible light. Unfortunately, overall water splitting using these oxynitrides has not been achieved, at least partly due to the relatively high defect densities in the bulk and at the surfaces of these materials. However, some of them do function as a building block for H_2 evolution in a two-step water splitting system (Z-scheme) under visible light.[19,20] These (oxy)nitrides are composed of transition metal cations of Ti^{4+}, Nb^{5+}, or Ta^{5+}, which have an empty d orbital. Because of their

† Accepted as part of the 2010 "Materials Chemistry of Energy Conversion Special Issue".

*Corresponding author. Tel.: +81-3-5841-1148. Fax: +81-3-5841-8838, E-mail: domen@chemsys.t.u-tokyo.ac.jp.

 Published on Web 09/14/2009

electronic band structure, d^{10}-semiconductors containing typical metal cations have an advantage as a photocatalyst, compared to materials with d^0 electronic configuration.[6,7] The top of the valence band in transition-metal oxides with a d^0 electronic configuration consists of O2p orbitals, whereas the bottom of the conduction band is composed of empty d orbitals of the transition metals. In typical metal oxides with a d^{10} electronic configuration, however, the bottom of the conduction band consists of hybridized s,p orbitals of the metals, although the valence band is essentially formed by O2p orbitals. The hybridized s,p orbitals have large dispersion, increasing the mobility of photogenerated electrons in the conduction band and promoting photocatalytic activity.[6,7]

(Oxy)nitrides with a d^{10} electronic configuration are therefore of interest as potentially efficient photocatalysts for overall water splitting. In evaluating such d^{10}-compounds according to this hypothesis, it was found that β-Ge_3N_4 loaded with RuO_2 nanoparticles functions as a photocatalyst for overall water splitting.[21−24] This was the first case involving a nonoxide photocatalyst for the cleavage of pure water. Since this discovery, the photocatalytic properties and effects of post-treatment to enhance the activity of Ge_3N_4 have been examined in detail.[22,23] The relationship between the structural characteristics and the photocatalytic performance of Ge_3N_4 has also been investigated.[24] Unfortunately, the band gap of β-Ge_3N_4 is about 3.8 eV, which is responsive only to ultraviolet light.[21,23] This forced us to search for a new d^{10} compound that can function under visible light.

In this article, the development of such a material is described, focusing on a solid solution of gallium nitride (GaN) and zinc oxide (ZnO). As schematically illustrated in Figure 1, photocatalytic overall water splitting on a semiconductor powder involves several steps. Among these, suppressing recombination between photogenerated electrons and holes in a photocatalyst is the most important to achieving the reaction. The effects of physicochemical properties on water splitting activity have been investigated for many metal-oxide photocatalysts,[2d,7] whereas little information is available for nonoxide photocatalysts. As the solid solution is the first successful example of achieving overall water splitting under visible light ($\lambda > 400$ nm) with good reproducibility,[25−40] it is a good example for studying such physicochemical effects on activity. From the viewpoint of solid-state materials chemistry, we would like to pay attention to the refinement of the base photocatalyst, although our recent study has revealed that the photocatalytic activity is significantly enhanced upon modification of nanostructured cocatalysts based on rhodium and chromium as H_2 evolution sites.[29−36] It is also noted that a similar wurtzite-type solid solution consisting of $ZnGeN_2$ and ZnO was recently reported as an active photocatalyst for visible-light-driven overall water splitting.[41−44] Physicochemical effects on photocatalytic activity of GaN−ZnO solid solutions, which will be mentioned below, can therefore be applicable to $ZnGeN_2$−ZnO solid solutions.

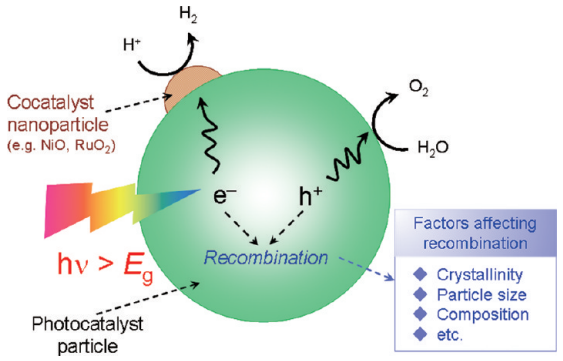

Figure 1. Schematic illustration of overall water splitting on a heterogeneous photocatalyst.

2. Initial Concept for Designing GaN−ZnO Solid Solutions

To devise a new d^{10}-(oxy)nitride with a visible light response, our initial focus was on gallium nitride (GaN), which has been studied extensively for application in light-emitting diodes and laser diodes.[45,46] Although GaN was confirmed to have potential for overall water splitting, its large band gap (ca. 3.4 eV) restricts its use of visible photons.[47−49] Nevertheless, we believed that this situation could be overcome by the following strategy. For II−VI semiconductors containing Zn^{2+} ions as a principal component (e.g., $ZnAl_2O_4$), it has been reported that p−d repulsion (e.g., O2p−Zn3d) shifts the valence-band maximum upward without affecting the conduction-band minimum.[50] Similarly, it was hypothesized that p−d repulsion may occur when a zinc(II) compound is incorporated into the GaN lattice, causing the top of the valence band formed by N2p atomic orbitals to rise to a higher potential energy (i.e., N2p−Zn3d repulsion), narrowing the band gap for GaN. Because both GaN and ZnO have wurtzite structures with similar lattice parameters,[51,52] a solid solution can be formed between the two (Figure 2). In this context, ZnO was chosen as a partner for GaN to form a solid solution with visible light response. The expected band structure of GaN−ZnO solid solution is illustrated in Figure 3.

Preparation of the solid solution was first attempted by nitriding a mixture of β-Ga_2O_3 and ZnO under a flow of ammonia at ~1223 K. As shown in Figure 4, the as-obtained products were yellow powders, depending on the preparation condition. The yellow color clearly indicates visible-light-absorption by this material, consistent with the initial hypothesis. Elemental analysis by inductive coupled plasma optical emission spectroscopy (ICP-OES) revealed that the ratios of Ga to N and Zn to O were close to 1, and that the nitrogen and oxygen concentrations increased with increasing gallium and zinc concentrations.[25] X-ray diffraction (XRD) analysis showed that the prepared material had a wurtzite structure similar to GaN and ZnO, and that the diffraction peaks were between those of GaN and ZnO (as will be discussed below in more detail). Based on these results, it was concluded that the obtained material was indeed a solid solution

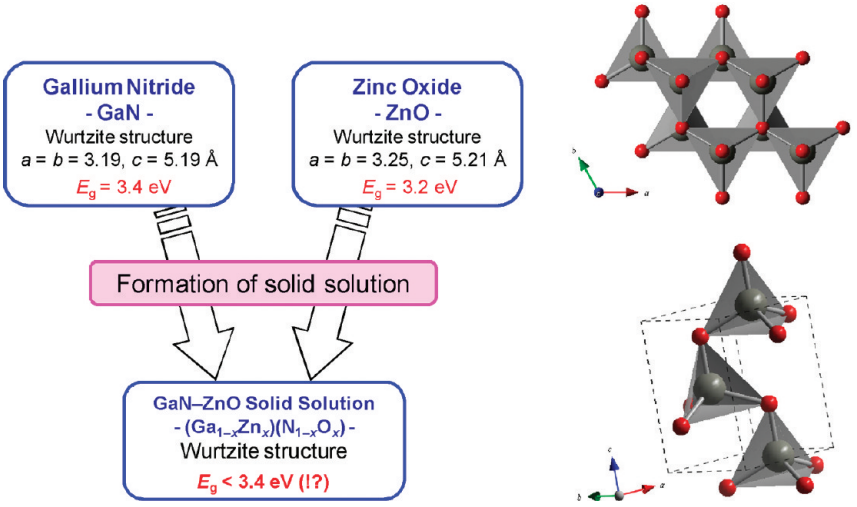

Figure 2. Crystal structure and lattice constants of GaN and ZnO.

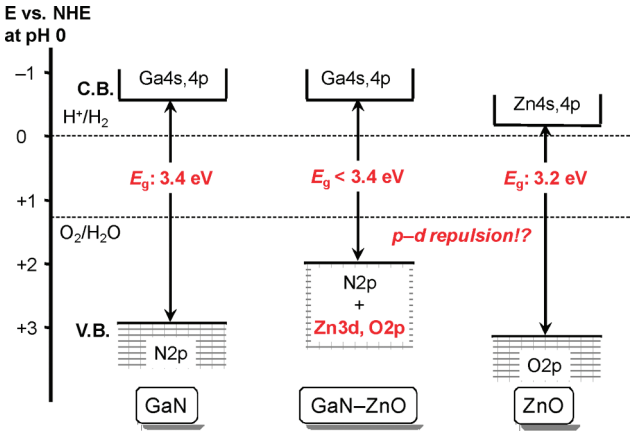

Figure 3. Schematic illustration of band structures of GaN, ZnO, and their solid solution.

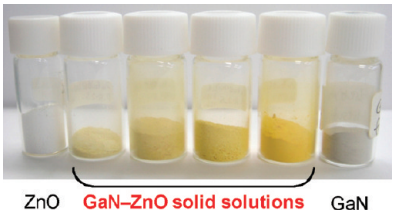

Figure 4. Photographs of GaN, ZnO, and $(Ga_{1-x}Zn_x)(N_{1-x}O_x)$ solid solutions.

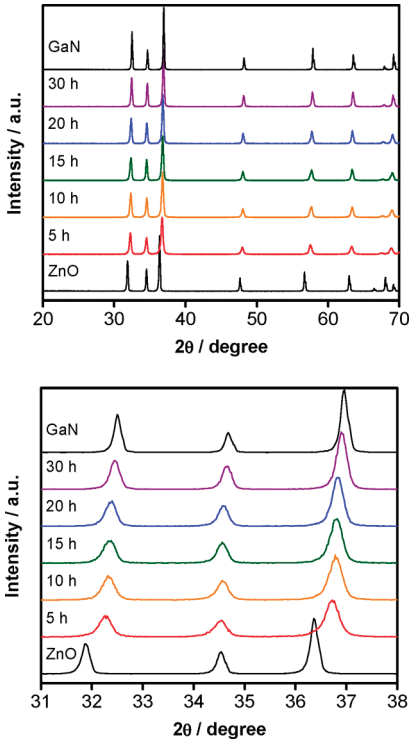

Figure 5. Powder XRD patterns of samples obtained by nitriding a mixture of β-Ga_2O_3 and ZnO (molar ratio Zn/Ga = 1) under a flow of NH_3 at 1123 K for several time periods. ZnO and GaN references were purchased from Kanto Chemicals and Mitsubishi Chemicals Co., respectively.

of GaN and ZnO (represented as $(Ga_{1-x}Zn_x)(N_{1-x}O_x)$ hereafter), and more systematic study was begun.

3. Effect of Nitridation Conditions

Thermal ammonolysis is a convenient technique for synthesizing particulate metal (oxy)nitrides from the corresponding precursors, and the physicochemical properties of the products can be controlled through appropriate adjustment of the preparation conditions.[15,18,24,53−57] In general, the functionality (e.g., photocatalytic activity) of a given material is strongly dependent on its physicochemical characteristics.[15,18,24,57] Therefore, investigating the relationship between the functionality and physicochemical characteristics of a material should provide useful information for further refinement of such systems. The physicochemical properties of $(Ga_{1-x}Zn_x)(N_{1-x}O_x)$ and the optimal preparation conditions were investigated in an attempt to improve the activity of the material for overall water splitting.[26]

Figure 5 shows XRD patterns from samples obtained by nitriding a mixture of β-Ga_2O_3 and ZnO (Zn/Ga = 1 by mole) at 1123 K for several periods. GaN and ZnO data are shown for comparison. A single hexagonal wurtzite phase similar to the GaN and ZnO was obtained for all

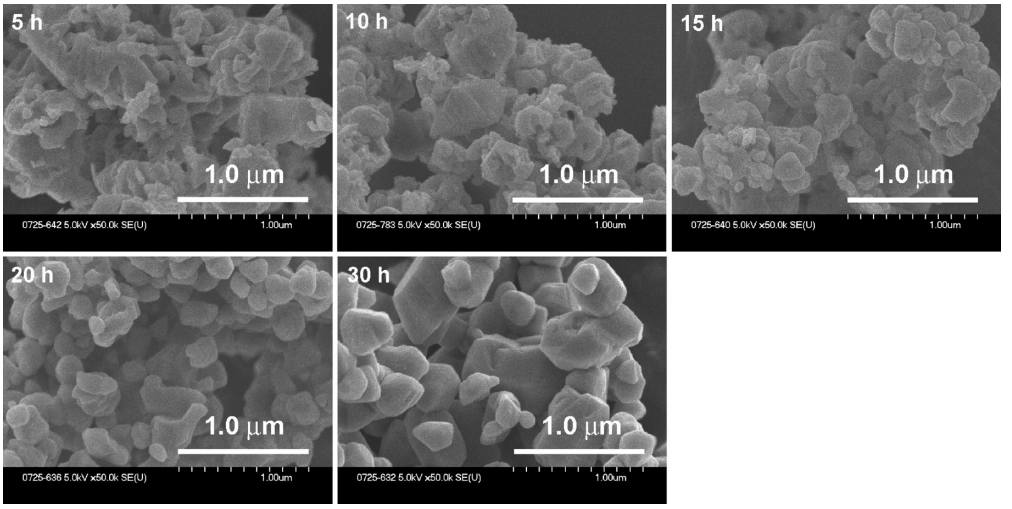

Figure 6. SEM images of samples obtained by nitriding a mixture of β-Ga_2O_3 and ZnO (molar ratio Zn/Ga = 1) under a flow of NH_3 at 1123 K for several time periods.

prepared samples, but nitridation for less than 5 h did not lead to the formation of the single wurtzite phase. In addition to the peaks assigned to the solid solution, some small peaks assigned to ZnO and $ZnGa_2O_4$ were observed in the nitridation products. The positions of the diffraction peaks shifted to higher angles (2θ) with increasing nitridation time, indicating that the obtained samples were not physical mixtures of GaN and ZnO phases, but rather solid solutions of GaN and ZnO. The zinc and oxygen concentration in the solid solution thus decreased with reduction of the ZnO content and subsequent volatilization of zinc in the solid solution due to exposure to a reductive atmosphere during nitridation. This peak shift is reasonable, as the ionic radius of Zn^{2+} (0.74 Å) is larger than that of Ga^{3+} (0.61 Å).[58] Thus, there was a linear relationship between the lattice constants (a and c) and the composition (x) of $(Ga_{1-x}Zn_x)(N_{1-x}O_x)$.[26]

Figure 6 shows scanning electron microscope (SEM) images of the same samples. Particles prepared by nitridation for less than 15 h were irregularly shaped, whereas those nitrided for longer periods became more regular and larger with increasing nitridation time. This change in particle shape agrees well with the XRD measurements, in which the peaks became stronger and narrower with increasing nitridation time (Figure 5). These measurements reveal that the crystallization of the nitridation products proceeds gradually from 5 to 30 h during nitridation at 1123 K. Transmission electron microscope (TEM) images and an electron diffraction pattern of $(Ga_{1-x}Zn_x)(N_{1-x}O_x)$ prepared by nitridation for 15 h are shown in Figure 7. The figure clearly reveals that the sample consisted primarily of well-crystallized submicrometer particles with a wurtzite structure, as indicated by the lattice fringe and electron diffraction patterns. Energy dispersive X-ray spectroscopy (EDS) analysis for each spot area (ca. 20 nm) revealed that the atomic composition of the material deviates from spot to spot, even in the same primary particle. Such nonuniformity in atomic composition is indicative of simultaneous diffusion of constituent ions of the starting mixtures (i.e., Ga^{3+}, Zn^{2+}, and O^{2-}) and nitridation at the solid−solid boundary between β-Ga_2O_3 and ZnO.

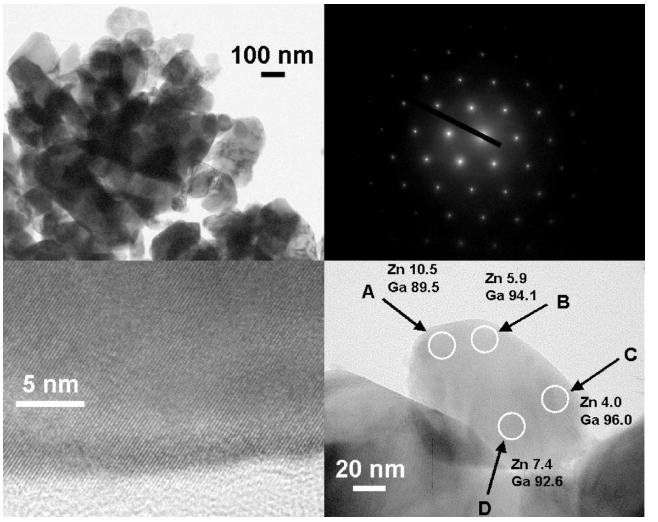

Figure 7. TEM images and an electron diffraction pattern of a sample obtained by nitriding a mixture of β-Ga_2O_3 and ZnO (molar ratio Zn/Ga=1) under a flow of NH_3 at 1123 K for 15 h. Results of EDS analysis are also shown.

UV−visible diffuse reflectance spectra for the same set of samples are shown in Figure 8A, along with GaN and ZnO data for comparison. As suggested from the photographs (Figure 4), the absorption edges of $(Ga_{1-x}Zn_x)$-$(N_{1-x}O_x)$ were at longer wavelengths than those of GaN or ZnO, but shifted to shorter wavelengths with increasing nitridation time. The band gap of the present samples was roughly estimated to be 2.6−2.8 eV, based on the onsets of the diffuse reflectance spectra, which were substantially smaller than those of GaN (3.4 eV) or ZnO (3.2 eV). Figure 8B shows the relationship between the estimated band gap energy and the ZnO concentration of $(Ga_{1-x}Zn_x)$-$(N_{1-x}O_x)$. Here, the band gap energy decreased with increasing ZnO concentration, indicating that the visible-light-response of $(Ga_{1-x}Zn_x)(N_{1-x}O_x)$ comes from the presence of ZnO in the crystal. The photoluminescence and photoluminescence excitation spectra of $(Ga_{1-x}Zn_x)(N_{1-x}O_x)$

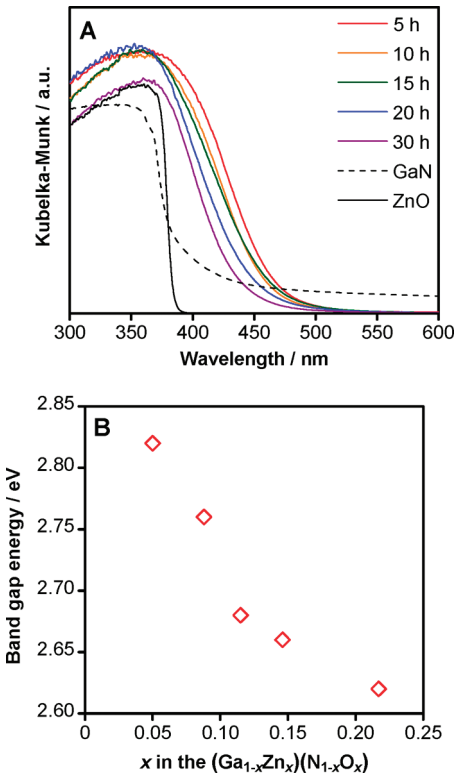

Figure 8. (A) Diffuse reflectance spectra of samples obtained by nitriding a mixture of β-Ga_2O_3 and ZnO (molar ratio Zn/Ga = 1) under a flow of NH_3 at 1123 K for several time periods. ZnO and GaN references were purchased from Kanto Chemicals and Mitsubishi Chemicals Co., respectively. (B) Relationship between band gap energies and ZnO concentration (x) of the $(Ga_{1-x}Zn_x)(N_{1-x}O_x)$.

with compositions of $x = 0.05-0.20$ (i.e., GaN-rich) measured at 10 K suggested that the visible light absorption of this material occurs via Zn-related acceptor levels.[59] This idea, however, contradicts our previous density functional theory (DFT) calculations, which indicate that the bottom of the conduction band for $(Ga_{1-x}Zn_x)(N_{1-x}O_x)$ is mainly composed of 4s and 4p orbitals of Ga, while the top of the valence band consists of N 2p orbitals followed by Zn 3d and O 2p orbitals.[2b] This idea remains valid for the solid solution with stoichiometric unit cells. For a dilute solid solution, however, it is natural to consider the local inhomogeneity of the Zn and O atom densities. In such circumstances, empty impurity levels appear just above the valence band, and/or filled impurity levels appear just below the conduction band. These impurity levels may explain the photoluminescence experimental results, and were characterized by our DFT calculations with nonstoichiometric unit cells. Very recently, Muckerman et al. and Huang et al. have studied the same material using theoretical calculations.[60] Their results are essentially identical to those obtained in our previous study.

The photocatalytic activity of as-prepared $(Ga_{1-x}Zn_x)(N_{1-x}O_x)$ for overall water splitting was negligible, regardless of the preparation conditions. However, the modification of $(Ga_{1-x}Zn_x)(N_{1-x}O_x)$ with nanoparticulate transition-metal oxides (e.g., NiO, RuO_2, or $Rh_{2-y}Cr_yO_3$) resulted in clearly observable H_2 and O_2 evolution.

Table 1. Effect of Nitridation Conditions on the Chemical Composition, Specific Surface Area, and Photocatalytic Activity for Overall Water Splitting under UV and Visible Light Irradiation ($\lambda > 300$ nm)

	nitridation conditions[a]				activity[c] (μmol h^{-1})	
entry	T (K)	time (h)	Zn/Ga atomic ratio[b]	specific surface area/$m^2 \cdot g^{-1}$	H_2	O_2
1	1123	5	0.28	7.9	2.5	1.5
2		10	0.17	7.4	8.7	4.1
3		15	0.13	7.4	29	14
4		20	0.10	6.7	20	9.2
5		30	0.05	5.8	14	6.9
6	1173	3	0.35	8.1	1.4	1.2
7		5	0.08	5.0	11	5.2
8		10	0.05	5.1	15	7.0
9		15	0.06	4.9	10	4.9
10		20	0.05	4.7	7.7	3.2
11	1223	1	0.29	8.3	3.9	1.8
12		3	0.07	5.3	14	6.9
13		5	0.06	5.0	15	7.4
14		10	0.04	3.5	11	5.0
15		15	0.04	3.7	4.5	2.0

[a] A mixture of β-Ga_2O_3 and ZnO (Zn/Ga = 1 by mole) was employed as a starting material. In all cases, a single wurtzite phase was observed in XRD measurements. [b] Estimated from EDX measurements. [c] Reaction conditions: catalyst, 0.3 g (1.5 wt % NiO loaded by impregnation with $Ni(NO_3)_2$ followed by calcination in air at 573 K for 1 h); reactant solution, pure water (420 mL); reaction vessel, Pyrex inner-irradiation-type; light source, high-pressure mercury lamp (450 W). Listed are average rates of H_2 and O_2 evolution after 5 h of reaction.

This modification involved the deposition of metal-oxide nanoparticles on the surface of the $(Ga_{1-x}Zn_x)(N_{1-x}O_x)$ as H_2 evolution sites. Table 1 lists the photocatalytic activity for overall water splitting using samples prepared under various nitridation conditions. Data including the chemical composition and specific surface area are also included in the table. A trade-off relationship between activity and nitridation conditions was observed; specifically, the activity increased, up to a certain point, as nitridation progressed, but further nitridation resulted in decreased activity. It also appeared that the activity was nearly independent of the specific surface area, unlike the behavior generally observed in metal-oxide photocatalysts.[7] Taking a series of samples prepared at 1123 K for different durations as an example, the largest increase in activity was obtained in the range between 5 and 15 h of nitridation (entries 1−3, Table 1), where the XRD peak became stronger and narrower (Figure 5) and the particle shape became more regular (Figure 6). The increase in activity with nitridation time was therefore considered to be associated with the crystallization of $(Ga_{1-x}Zn_x)(N_{1-x}O_x)$, which reduced the number of defects acting as recombination centers between photogenerated electrons and holes. Nitridation for longer than 15 h had reduced the activity of the catalyst from its maximum value, which seemed to be attributable to a decrease in zinc concentration at the surface of the catalysts. X-ray photoelectron spectroscopy (XPS) and EDX analysis revealed that the zinc concentration in the $(Ga_{1-x}Zn_x)(N_{1-x}O_x)$ decreased with increasing nitridation time, and the degree of the decrease was more prominent at the surface than in the bulk.[26] Under the present nitridation conditions, ZnO species in $(Ga_{1-x}Zn_x)(N_{1-x}O_x)$ were reduced to zinc

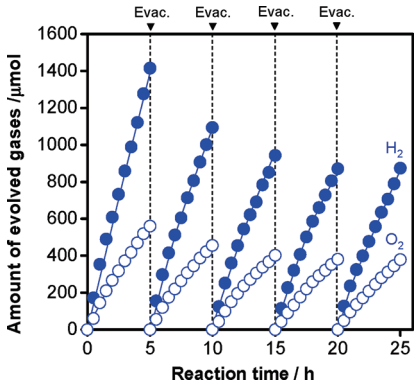

Figure 9. Typical time course of overall water splitting under UV and visible irradiation ($\lambda > 300$ nm) on 3.5 wt % RuO_2-loaded $(Ga_{1-x}Zn_x)(N_{1-x}O_x)$ (entry 3, see Table 1). Catalyst (0.3 g); reactant solution, pure water (390 mL); light source, high-pressure mercury lamp (450 W); inner-irradiation-type Pyrex reaction vessel.

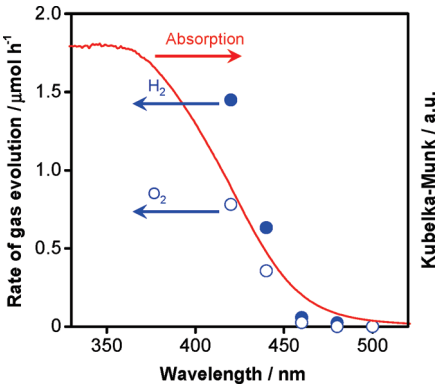

Figure 10. Dependence of the rates of H_2 and O_2 evolution by 5 wt % RuO_2-loaded $(Ga_{1-x}Zn_x)(N_{1-x}O_x)$ (entry 3, see Table 1) on the cutoff wavelength of the incident light. Catalyst (0.3 g); an aqueous solution adjusted to pH 3 by H_2SO_4 (200 mL); light source, xenon lamp (300 W) attached with a cutoff filter; top-irradiation-type Pyrex reaction vessel.

metal, which volatized to zinc vapor. The remnant oxygen was removed as H_2O, but not completely. This situation resulted in vacancies at zinc sites at the catalyst surface, which acted as recombination centers between photogenerated electrons and holes. This idea is supported by the difficulty of preparing a high-activity catalyst at temperatures above 1173 K (Table 1). This was attributed to the formation of zinc- and/or oxygen-related defects at the $(Ga_{1-x}Zn_x)(N_{1-x}O_x)$ surface at such high temperatures. Conversely, it was difficult to obtain a single phase of $(Ga_{1-x}Zn_x)(N_{1-x}O_x)$ at temperature below 1073 K, even with extended nitridation periods, probably because of the poor reactivity of the starting materials with NH_3 gas at lower temperatures. Thus, the optimal temperature for preparation of $(Ga_{1-x}Zn_x)(N_{1-x}O_x)$ is considered to be 1123 K.

A typical time course of overall water splitting on $(Ga_{1-x}Zn_x)(N_{1-x}O_x)$, prepared at the above-optimized condition under irradiation by UV and visible light ($\lambda >$ 300 nm) is shown in Figure 9. In this case, RuO_2 nanoparticles were employed as a promoter. The gas phase was evacuated every 5 h, and the reaction was allowed to proceed for a total of 25 h to evaluate stability. At the initial stage of the reaction, the evolution ratio of H_2 to O_2 was slightly larger than that expected from the stoichiometry, and the activity decreased with increasing reaction time. Nevertheless, the activity stabilized in the fourth run, at an H_2/O_2 ratio of 2. The total evolution of H_2 and O_2 after 25 h was 7.48 mmol, substantially exceeding the total amount of catalyst (3.56 mmol) employed for the reaction. It has also been confirmed by XRD, XPS, and X-ray absorption fine-structure spectroscopy (XAFS) that the crystal structure of the catalyst and the valence state of both the surface and bulk did not change, even after reaction for 3 days at the optimal reaction conditions.[32] Figure 10 shows the dependence of the rate of H_2 and O_2 evolution on the wavelength of incident light. The H_2 and O_2 evolution rates both decreased as the cutoff wavelength increased. The longest wavelength available for the water splitting reaction was 460 nm, corresponding to the absorption edge of the catalyst. This result clearly indicates that the reaction proceeded photocatalytically through light absorption by $(Ga_{1-x}Zn_x)(N_{1-x}O_x)$. It has been reported that O_2 evolution occurs on a ZnO electrode as a result of degradation when employed as a photoanode for water oxidation in a photoelectrochemical cell.[61] Interestingly, it was confirmed through ^{18}O-isotopic H_2O cleavage experiments that the O_2 evolution on $(Ga_{1-x}Zn_x)(N_{1-x}O_x)$ was due to water oxidation, with the XRD pattern of the sample remaining unchanged after the reaction.[25] Control experiments showed no gas evolution in the absence of either a photocatalyst or a light source. These results lead us to conclude that $(Ga_{1-x}Zn_x)(N_{1-x}O_x)$ functions as a stable photocatalyst for overall water splitting under visible light.

For nonoxide photocatalysts, it is important to note the effect of self-decomposition by photogenerated holes in the valence band of the material, since this process competes with the water photooxidation reaction (eq 3). In overall water splitting using $(Ga_{1-x}Zn_x)(N_{1-x}O_x)$ modified with cocatalysts, a negligible amount of N_2 evolution ($\sim$10 μmol) was detected in the initial stage of the reaction (first 1−2 h). This was attributed to the oxidation of N^{3-} species near the $(Ga_{1-x}Zn_x)(N_{1-x}O_x)$ surface to N_2, as has been observed for other (oxy)nitride photocatalysts.[11,15,17,18,19a,20−24,57,62]

$$2N^{3-} + 6h^+ \rightarrow N_2 \qquad (4)$$

However, the production of N_2 was completely suppressed as the reaction proceeded, indicative of good stability of the material. This behavior is very different from conventional nonoxide photocatalysts such as cadmium sulfide (CdS), where photogenerated holes oxidize the material itself under overall water splitting conditions without participating in water oxidation due to the inherent instability of the material.[10]

4. Effect of Starting Materials

In a typical synthesis, $(Ga_{1-x}Zn_x)(N_{1-x}O_x)$ can be obtained by nitriding a mixture of β-Ga_2O_3 and ZnO at temperatures higher than 1123 K under a flow of NH_3, as

Table 2. Effect of Starting Materials on the Preparation of $(Ga_{1-x}Zn_x)(N_{1-x}O_x)$ and Photocatalytic Activity for Overall Water Splitting under Visible Light Irradiation ($\lambda > 400$ nm)

			Zn/Ga atomic ratio		activity[c] (μmol h^{-1})	
entry	starting material	crystal phase in product[a]	in starting material	in product[b]	H_2	O_2
1	β-Ga_2O_3 + ZnO	solid solution	1.0	0.13	270	134
2	α-Ga_2O_3 + ZnO	solid solution	1.0	0.14	316	162
3	γ-Ga_2O_3 + ZnO	solid solution	1.0	0.13	32	16
4	GaN + ZnO	GaN	1.0	no data	no data	no data
5	$ZnGa_2O_4$	solid solution	0.5	0.25	<0.5	0
6	$ZnGa_2O_4$ + ZnO	solid solution	1.0	0.29	213	111
7	β-Ga_2O_3 + Zn	solid solution + $ZnGa_2O_4$ + etc.	1.0	no data	no data	no data

[a] Determined by XRD measurements. [b] Estimated from EDX measurements. [c] Reaction conditions: catalyst, 0.3 g (1 wt % Rh and 1.5 wt % Cr loaded by impregnation with $Na_3RhCl_6 \cdot 2H_2O$ and $Cr(NO_3)_3 \cdot 9H_2O$ followed by calcination in air at 623 K for 1 h); reactant solution, aqueous solution adjusted to pH 4.5 by H_2SO_4 (370 mL); reaction vessel, Pyrex inner-irradiation-type; light source, high-pressure mercury lamp (450 W). Listed are steady rates of H_2 and O_2 evolution in 5 h of reaction.

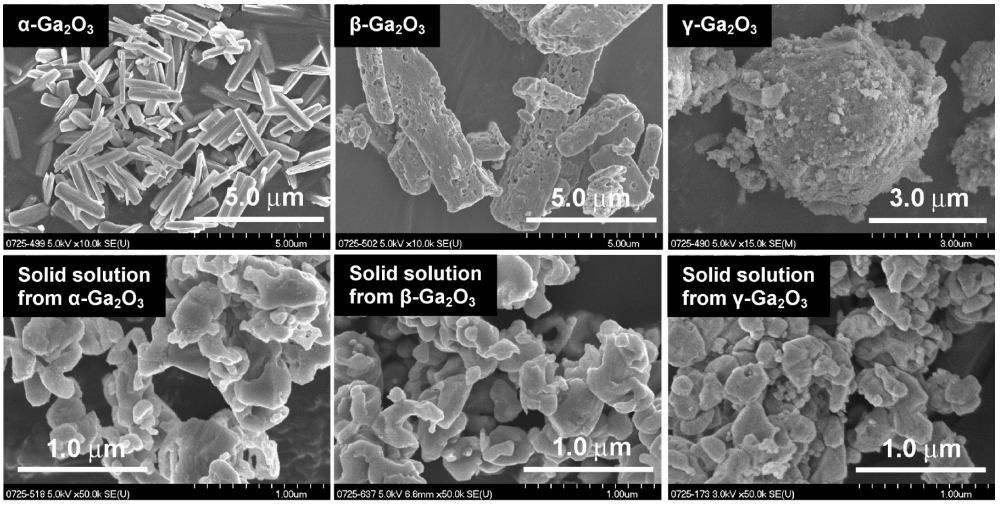

Figure 11. SEM images of $(Ga_{1-x}Zn_x)(N_{1-x}O_x)$ obtained by nitriding a mixture of ZnO and either (a) α-Ga_2O_3, (b) β-Ga_2O_3, or (c) γ-Ga_2O_3. Data for the Ga polymorphs are also shown.

described above. It is essential to understand the detailed effects of the starting materials on nitridation in order to develop a highly active photocatalyst. It is generally known that the starting material affects the physicochemical properties (e.g., crystallinity, surface structure, and composition) of the final product that play a crucial role in determining the activity.[5−7]

The effects of the starting materials on physicochemical and photocatalytic properties of the resulting $(Ga_{1-x}Zn_x)(N_{1-x}O_x)$ have thus been systematically investigated.[39,40] Table 2 summarizes the results of preparation and the photocatalytic activity of the final products using various Ga and Zn compounds. First of all, α-, β-, and γ-Ga_2O_3 and GaN were tested as Ga-sources for synthesizing $(Ga_{1-x}Zn_x)(N_{1-x}O_x)$. The use of α- and γ-Ga_2O_3 as the starting material resulted in successful production of $(Ga_{1-x}Zn_x)(N_{1-x}O_x)$ (entries 2 and 3), as in the case of β-Ga_2O_3 (entry 1). Despite the similarity in XRD patterns, specific surface area, and chemical composition, the activity of the sample prepared using γ-Ga_2O_3 was 1 order of magnitude lower than that of those derived from α- and β-Ga_2O_3.[40] One possible explanation for this low activity is that the γ-derived sample had a rough surface structure. Figure 11 shows SEM images of $(Ga_{1-x}Zn_x)(N_{1-x}O_x)$ prepared using various Ga_2O_3 polymorphs, whose SEM data are also displayed. $(Ga_{1-x}Zn_x)(N_{1-x}O_x)$ prepared using α- and β-Ga_2O_3 exhibited similar morphology with a relatively smooth surface structure. On the other hand, the sample prepared using γ-Ga_2O_3 contained fine particles and structural imperfections, although some well-crystallized particles were also observed. Such surface-roughness can function as traps for photogenerated electrons and holes, reducing the efficiency of photocatalysis. γ-Ga_2O_3 consists of agglomerates several micrometers in size, composed of aggregated primary particles smaller than 50 nm. Therefore, it appears that the contact of γ-Ga_2O_3 with ZnO in the mixture of starting materials becomes inevitably less intimate than when using α- or β-Ga_2O_3. This situation would result in morphological roughness of the resulting $(Ga_{1-x}Zn_x)(N_{1-x}O_x)$. This idea was further supported by another experiment, in which the effect of the Zn/Ga molar ratio in the starting material was investigated, as will be discussed below. On the other hand, nitridation of GaN and ZnO in the same manner did not lead to the production of $(Ga_{1-x}Zn_x)(N_{1-x}O_x)$ (entry 4). The XRD pattern of the obtained product was identical to that of the starting GaN. This indicates that the ZnO in the starting material volatized by exposure to a reductive atmosphere derived from NH_3 at high temperatures,

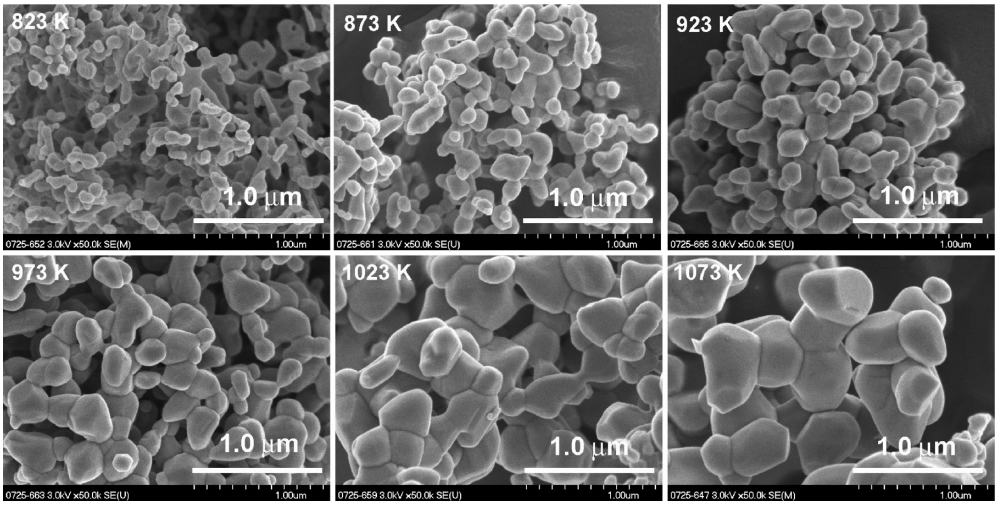

Figure 12. SEM images of ZnO (purchased from Wako Pure Chemicals Co.) powder calcined in air for 2 h at different temperatures.

without reacting with GaN under the present nitridation conditions. This suggests that, at least under the present nitridation conditions, the formation of $(Ga_{1-x}Zn_x)(N_{1-x}O_x)$ does not take place at the solid−solid boundary between GaN and ZnO, and that the incorporation of ZnO into the GaN matrix to form $(Ga_{1-x}Zn_x)(N_{1-x}O_x)$ takes place when Ga−O bonds are cleaved and converted to Ga−N bonds during nitridation.

$ZnGa_2O_4$ was also found to be a useful starting material for $(Ga_{1-x}Zn_x)(N_{1-x}O_x)$, but the final product exhibited little photocatalytic activity (entry 5).[39] The addition of ZnO was essential for preparing a high-activity catalyst (entry 6). XRD analysis and SEM observation revealed that the sample prepared from $ZnGa_2O_4$ had relatively low crystallinity and many structural imperfections, compared to an analogous sample prepared with an addition of ZnO. This was the probable cause of its negligible activity, and strongly suggests an important role of ZnO in the preparation of $(Ga_{1-x}Zn_x)(N_{1-x}O_x)$. The importance of ZnO was further indicated when nitridation of a mixture of metallic Zn powder and β-Ga_2O_3 in a similar manner did not lead to the formation of $(Ga_{1-x}Zn_x)(N_{1-x}O_x)$ (entry 7). XRD analysis showed that $ZnGa_2O_4$ and some other impurity phases were contained in the nitridation products in addition to the solid solution phase, and the intensity of the peaks assigned to the solid solution was much lower than in the sample prepared using ZnO.[40] This result indicates that the changes in physicochemical properties of the resulting $(Ga_{1-x}Zn_x)(N_{1-x}O_x)$ are derived not from metallic Zn but from ZnO, suggesting that ZnO in the starting material facilitated the formation of $(Ga_{1-x}Zn_x)(N_{1-x}O_x)$.

5. Effect of ZnO Particle Size and the Zn/Ga Molar Ratio in Starting Materials

More detailed investigation on the ZnO-effect revealed that the ZnO particle size and the ratio of Zn/Ga in the starting materials both play an important role in producing $(Ga_{1-x}Zn_x)(N_{1-x}O_x)$ with high photocatalytic activity.[40] To examine the effect of ZnO particle size, we simply calcined commercially available ZnO nanoparticles (ca. 20 nm) in air at different temperatures. This produced ZnO particles of different sizes, as shown in Figure 12.[40] Figure 13 shows the XRD patterns of samples obtained by nitriding a mixture of β-Ga_2O_3 and ZnO of different particle sizes (Zn/Ga = 1 by mole), along with the GaN and ZnO data for comparison. The nitridation temperature and time were fixed at 1123 K and 15 h, respectively, in order to eliminate any effects other than the particle size of ZnO. All prepared samples had a single phase of hexagonal wurtzite, similar to the GaN and ZnO references. The positions of the diffraction peaks for all prepared samples were located between those of the GaN and ZnO references, indicating that the obtained samples were not a physical mixture of GaN and ZnO phases but rather solid solutions of GaN and ZnO. Although there was no significant difference in the diffraction peak positions of the samples, the diffraction peaks tended to become somewhat broad and asymmetric with increasing ZnO particle size. Samples prepared using ZnO calcined at higher temperatures (i.e., having larger particle size) had a small shoulder on the low-angle side of the diffraction peak (ca. $2\theta = 36.7$). This is assignable to $(Ga_{1-x}Zn_x)(N_{1-x}O_x)$ containing a relatively large amount of zinc and

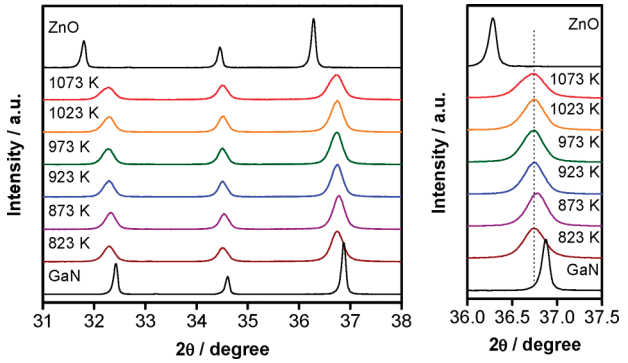

Figure 13. XRD patterns of $(Ga_{1-x}Zn_x)(N_{1-x}O_x)$ obtained by nitriding a mixture of β-Ga_2O_3 and ZnO (Zn/Ga = 1 by mole) calcined at different temperatures at 1123 K for 15 h. Data for ZnO and GaN are also shown.

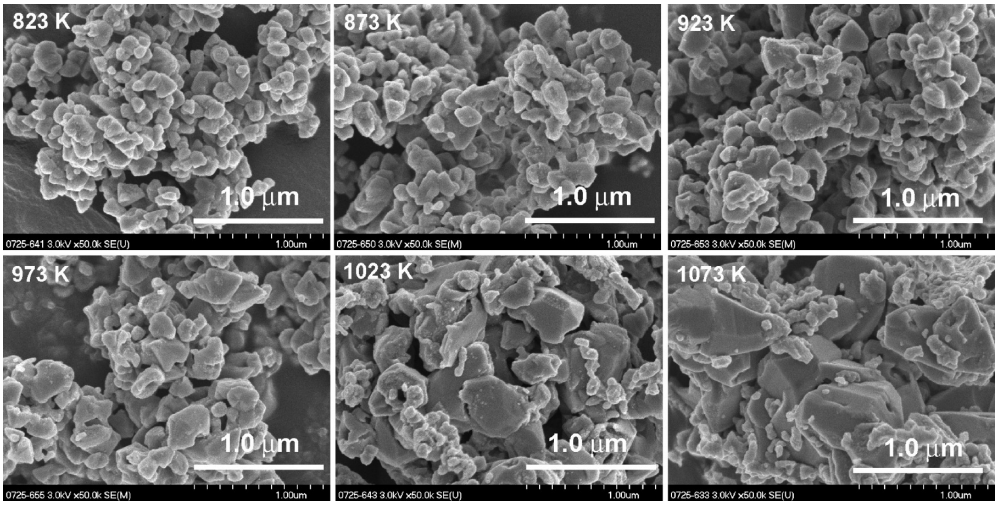

Figure 14. SEM images of $(Ga_{1-x}Zn_x)(N_{1-x}O_x)$ obtained by nitriding a mixture of β-Ga_2O_3 and ZnO (Zn/Ga = 1 by mole) calcined at different temperatures at 1123 K for 15 h.

oxygen, because the diffraction peaks shift to a lower angle (2θ) when Ga^{3+} cations in the $(Ga_{1-x}Zn_x)(N_{1-x}O_x)$ crystal are substituted by Zn^{2+} cations, which have a larger ionic radius than Ga^{3+}.[58] This indicates that the composition of $(Ga_{1-x}Zn_x)(N_{1-x}O_x)$ becomes less uniform with increasing zinc and oxygen concentration at increased ZnO calcination temperatures. It is thus clear that more intimate contact between β-Ga_2O_3 and ZnO in starting mixtures is essential for producing $(Ga_{1-x}Zn_x)(N_{1-x}O_x)$ of homogeneous composition.

The SEM images of the same samples are shown in Figure 14. Although each sample was nitrided under a flow of NH_3 at the same nitridation conditions, the morphologies of samples prepared using ZnO with various particle sizes were clearly different from each other. When ZnO calcined at 823 K was used, large agglomerates consisting of primary particles of about 100−200 nm in size were observed, and the primary particle size was relatively constant. However, with increasing ZnO calcination temperature, the primary particles became larger and acquired an irregular shape. This was in good agreement with XRD measurements, which revealed that the diffraction peaks became broad and asymmetric as the calcination temperature of ZnO increased (Figure 13). As the starting ZnO was calcined at higher temperatures, the particle size of ZnO increased (Figure 12), making it difficult to make good contact with the β-Ga_2O_3. As a result, irregular-shaped products would be obtained when ZnO with a relatively large size is used as a starting material, consistent with observations of cases using Ga_2O_3 polymorphs as starting materials.

The bulk atomic compositions for $(Ga_{1-x}Zn_x)(N_{1-x}O_x)$ prepared using ZnO of different particle sizes were investigated by EDX. The average atomic compositions and the standard deviations are summarized in Table 3. The ZnO concentration tended to increase with ZnO calcination temperature, and the standard deviation of the composition increased, in good agreement with the XRD results. As mentioned in the previous section, a decrease in ZnO concentration of $(Ga_{1-x}Zn_x)(N_{1-x}O_x)$ was caused by a reduction of the ZnO content and subsequent volatilization of zinc in the solid solution due to exposure to a reductive atmosphere during nitridation, and because the volatilization of zinc takes place more easily on the surface of the solid solution than in the bulk. Therefore, the increasing ZnO concentration of $(Ga_{1-x}Zn_x)(N_{1-x}O_x)$ with increasing ZnO calcination temperature indicates that $(Ga_{1-x}Zn_x)(N_{1-x}O_x)$ with larger particle sizes had less probability of contact with NH_3 during nitridation. In $(Ga_{1-x}Zn_x)(N_{1-x}O_x)$ prepared using ZnO calcined at higher temperatures, it appears that ZnO in the material bulk can avoid being reduced by NH_3 gas during nitridation, because NH_3 gas does not reach the material bulk. As a result, relatively high zinc and oxygen content would remain in the $(Ga_{1-x}Zn_x)(N_{1-x}O_x)$ after nitridation, if larger ZnO was used as a starting material. The increase in the standard deviation of the composition with calcination temperature of ZnO can be explained by less intimate contact between β-Ga_2O_3 and ZnO in the starting mixtures, as mentioned above.

Table 3. Atomic Composition and Its Standard Deviation for $(Ga_{1-x}Zn_x)(N_{1-x}O_x)$ Prepared by Nitriding a Mixture of β-Ga_2O_3 and ZnO Calcined at Various Temperatures

calcination temperature of ZnO[a]/K	Zn/Ga atomic ratio[b]	standard deviation in the composition
823	0.11	1.1
873	0.10	1.9
923	0.11	2.4
973	0.14	2.5
1023	0.18	3.3
1073	0.28	14

[a] Calcined in air for 2 h. [b] Estimated from EDX measurements.

If this is the case, increasing the ratio of ZnO to Ga_2O_3 in the starting material would facilitate the formation of $(Ga_{1-x}Zn_x)(N_{1-x}O_x)$ crystal, even when larger ZnO particles are employed. Figure 15 shows SEM images of samples obtained by nitriding a mixture of ZnO of different sizes and β-Ga_2O_3 with various Zn/Ga starting ratios. In the samples prepared from ZnO calcined at 1073

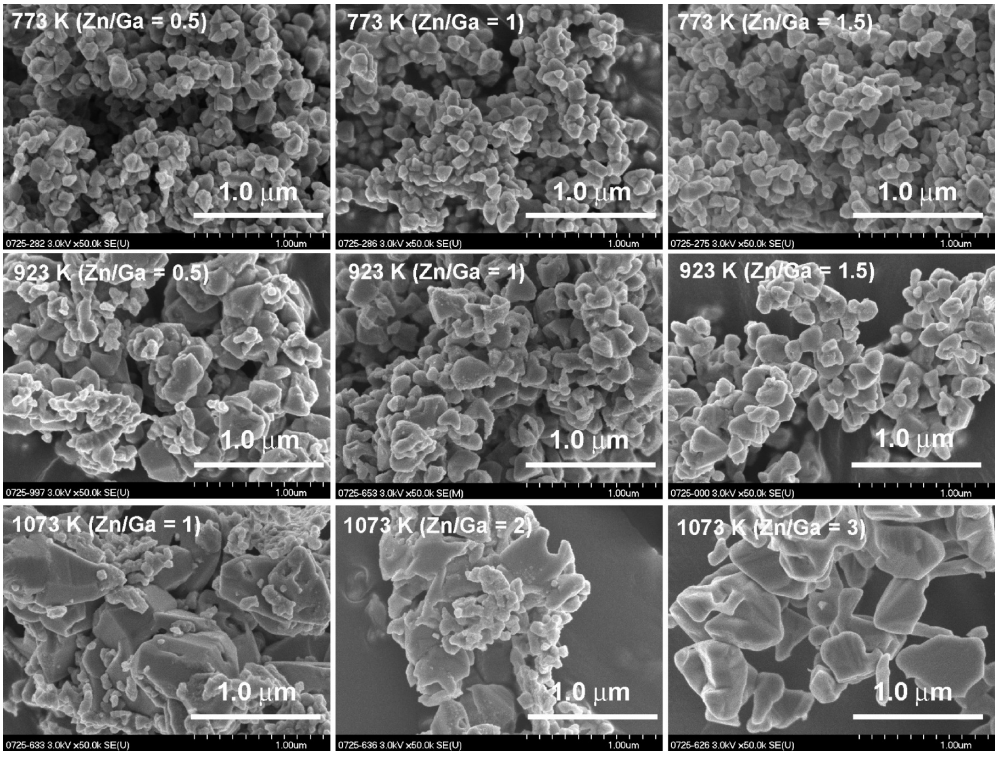

Figure 15. SEM images of $(Ga_{1-x}Zn_x)(N_{1-x}O_x)$ obtained by nitriding a mixture of β-Ga_2O_3 and ZnO calcined at different temperatures at 1123 K for 15 h with different Zn/Ga ratios in starting materials.

Table 4. Dependence of the photocatalytic activity of $(Ga_{1-x}Zn_x)(N_{1-x}O_x)$ for overall water splitting under visible light irradiation ($\lambda > 400$ nm) on ZnO calcination temperature and the Zn/Ga molar ratio in the starting material

		Zn/Ga atomic ratio		activity[c] (μmol h^{-1})	
entry	ZnO calcination temperature[a] (K)	in starting material	in product[b]	H_2	O_2
1	773	0.5	0.12	6	5
2	773	0.75	0.12	26	14
3	773	1	0.12	65	39
4	773	1.25	0.11	50	27
5	773	1.5	0.13	83	46
6	923	0.5	0.16	24	12
7	923	0.75	0.13	204	100
8	923	1	0.11	320	162
9	923	1.25	0.10	325	164
10	923	1.5	0.09	269	137
11	1073	1	0.29	144	73
12	1073	2	0.18	247	124
13	1073	3	0.06	60	30

[a] Calcined in air for 2 h. [b] Estimated from EDX measurements. [c] Reaction conditions: catalyst, 0.3 g (1 wt % Rh and 1.5 wt % Cr loaded by impregnation with $Na_3RhCl_6 \cdot 2H_2O$ and $Cr(NO_3)_3 \cdot 9H_2O$ followed by calcination in air at 623 K for 1 h); reactant solution, aqueous solution adjusted to pH 4.5 by H_2SO_4 (370 mL); reaction vessel, Pyrex inner-irradiation-type; light source, high pressure mercury lamp (450 W). Listed are steady rates of H_2 and O_2 evolution in 5 h of reaction.

(the largest size) and 923 K (the medium size), it was clear that more complete crystallization occurred at increased Zn/Ga ratios. This was further confirmed by XRD measurements, which revealed that the diffraction peaks become narrower and sharper as the Zn/Ga ratio was increased (data not shown here). In the samples prepared from the smallest ZnO particles (calcined at 773 K), on the other hand, no appreciable crystal growth was identified, even at high Zn/Ga ratios. It is known that ZnO can be reduced to metallic zinc upon exposure to a reducing atmosphere. Metallic zinc thus-formed in this process would convert to the liquid phase at temperatures between 700 and 1180 K.[63] We had therefore expected ZnO to be a useful flux under nitridation conditions, and to promote the crystallization of the final $(Ga_{1-x}Zn_x)(N_{1-x}O_x)$.[26] However, the lack of any promotional effect from the smallest ZnO suggests a different role(s) of ZnO in the nitridation process. If ZnO functions as a kind of flux, physicochemical properties of the nitridation products should be independent of the size of the ZnO particle. Interestingly, the particle size of the ZnO tended to determine that of the $(Ga_{1-x}Zn_x)(N_{1-x}O_x)$, and the crystallization of $(Ga_{1-x}Zn_x)(N_{1-x}O_x)$ seems to result in a decrease in ZnO concentration. Such behavior was not observed when the particle size of Ga_2O_3 was changed.[40] The mechanism by which $(Ga_{1-x}Zn_x)(N_{1-x}O_x)$ is formed therefore appears to be complicated and is now under further investigation. In situ XAFS is one possible approach to elucidating the formation mechanism.[64] Further investigations are required to clarify the role(s) of ZnO in the synthesis of $(Ga_{1-x}Zn_x)(N_{1-x}O_x)$.

Table 4 lists the photocatalytic activities of samples prepared with different sizes of ZnO and ratios of Zn/Ga, along with the atomic compositions. In a series of samples prepared using the medium- and largest-size ZnO, the activity increased with increasing Zn/Ga ratio up to a certain value, beyond which it then began to decline. The activity increase was due to crystallization of $(Ga_{1-x}Zn_x)(N_{1-x}O_x)$, which reduced the density of defects acting as recombination centers between photogenerated electrons

and holes. On the other hand, the drop in activity was likely due to a decrease in the ZnO concentration (x). This relationship is consistent with the findings above, in that the activity of $(Ga_{1-x}Zn_x)(N_{1-x}O_x)$ for overall water splitting is strongly dependent on the crystallinity and ZnO concentration of the material. This was also the case when a mixture of ZnO and $ZnGa_2O_4$ was employed as the starting material.[39] However, the exceptionally low activity of the samples prepared from the smallest ZnO particles (entries 1−5) has yet to be completely clarified. Presumably, there remain significant amounts of defect sites in the particles, because of the lower degree of crystallization. The importance of starting materials has been also reported for $ZnGeN_2$−ZnO solid solutions.[44] In that case, improving the homogeneity and reducing the defect density of the material contribute directly to activity-enhancement, similar to GaN−ZnO solid solutions.

6. Conclusions and Future Outlook

Preparation of $(Ga_{1-x}Zn_x)(N_{1-x}O_x)$ solid solutions as visible-light-driven photocatalysts for overall water splitting was reviewed. The material can be readily prepared by nitriding a mixture of ZnO and an appropriate Ga-source at temperatures above 1123 K under a flow of NH_3. The addition of ZnO to the starting material promotes crystallization of $(Ga_{1-x}Zn_x)(N_{1-x}O_x)$ and controls the zinc concentration, thereby improving activity. By adjusting the nitridation condition and the ratio of ZnO to the Ga source, it is possible to obtain a material with optimal crystallinity and atomic composition for overall water splitting under visible light.

The apparent quantum efficiency of the optimized $(Ga_{1-x}Zn_x)(N_{1-x}O_x)$ catalyst is at most on the order of several percent in the visible light region, indicating that more than 90% of photogenerated carriers recombine before reacting with water molecules. Thus, there remains substantial room for improvement. Another challenge to be addressed for this material is that it can absorb light only with wavelength shorter than 500 nm (corresponding to the blue part of solar spectrum). It was experimentally confirmed that $(Ga_{1-x}Zn_x)(N_{1-x}O_x)$ with a relatively high ZnO concentration ($x \approx 0.5$) and an absorption edge at 520 nm (band gap of ca. 2.4 eV) can be prepared through appropriate control of the preparation conditions and choice of starting materials. However, the activity of these high ZnO concentration samples is still low, compared to $(Ga_{1-x}Zn_x)(N_{1-x}O_x)$ with $x < 0.2$, which exhibits relatively high activity. Another possible approach is to make a solid solution of $(Ga_{1-x}Zn_x)$-$(N_{1-x}O_x)$ and indium nitride (InN), which is believed to have a very low band gap (< 1 eV).[65] Our preliminary study was successful in the synthesis of a mixed-oxynitride containing Ga, Zn, and In.[66] However, further refinement of the preparation method is required in this system in order to increase the crystallinity.

Acknowledgment. The research described herein was supported by the Core Research for Evolutional Science and Technology (CREST) and Solution Oriented Research for Science and Technology (SORST) programs of the Japan Science and Technology Corporation (JST). Acknowledgement is also extended to the 21st Century Center of Excellence (COE) and the Research and Development in a New Interdisciplinary Field Based on Nanotechnology and Materials Science programs of the Ministry of Education, Culture, Sports, Science and Technology (MEXT) of Japan. K.M. gratefully acknowledges the support of a Japan Society for the Promotion of Science (JSPS) Fellowship.

References

(1) Fujishima, A.; Honda, K. *Nature* **1972**, *238*, 37–38.
(2) (a) Lee, J. S. *Catal. Surv. Asia* **2005**, *9*, 217–227. (b) Maeda, K.; Teramura, K.; Saito, N.; Inoue, Y.; Kobayashi, H.; Domen, K. *Pure Appl. Chem.* **2006**, *78*, 2267–2276. (c) Maeda, K.; Domen, K. *J. Phys. Chem. C* **2007**, *111*, 7851–7861. (d) Kudo, A.; Miseki, Y. *Chem. Soc. Rev.* **2009**, *38*, 253–278.
(3) Domen, K.; Naito, S.; Soma, M.; Onishi, T.; Tamaru, K. *J. Chem. Soc., Chem. Commun.* **1980**, 543–544.
(4) Kim, H. G.; Hwang, D. W.; Kim, J.; Kim, Y. G.; Lee, J. S. *Chem. Commun.* **1999**, 1077–1078.
(5) Kato, H.; Asakura, K.; Kudo, A. *J. Am. Chem. Soc.* **2003**, *125*, 3082–3089.
(6) Sato, J.; Saito, N.; Nishiyama, H.; Inoue, Y. *J. Phys. Chem. B* **2001**, *105*, 6061–6063.
(7) Sato, J.; Kobayashi, H.; Ikarashi, K.; Saito, N.; Nishiyama, H.; Inoue, Y. *J. Phys. Chem. B* **2004**, *108*, 4369–4369.
(8) We define a photocatalyst that contains such transition metal cations (e.g., Ti^{4+}, Nb^{5+}, or Ta^{5+}) as a "d^0 electronic configuration" photocatalyst, whereas photocatalysts that contain typical metal cations (e.g., Ga^{3+} and Ge^{4+}) with a filled d orbital are defined as "d^{10} electronic configuration" photocatalysts.
(9) Scaife, D. E. *Solar Energy* **1980**, *25*, 41–54.
(10) (a) Williams, R. *J. Chem. Phys.* **1960**, *32*, 1505–1514. (b) Ellis, A. B.; Kaiser, S. W.; Bolts, J. M.; Wrighton, M. S. *J. Am. Chem. Soc.* **1977**, *99*, 2839–2848.
(11) Hitoki, G.; Takata, T.; Kondo, J. N.; Hara, M.; Kobayashi, H.; Domen, K. *Chem. Commun.* **2002**, 1698–1699.
(12) Hara, M.; Nunoshige, J.; Takata, T.; Kondo, J. N.; Domen, K. *Chem. Commun.* **2003**, 3000–3001.
(13) Maeda, K.; Terashima, H.; Kase, K.; Higashi, M.; Tabata, M.; Domen, K. *Bull. Chem. Soc. Jpn.* **2008**, *81*, 927–937.
(14) Maeda, K.; Terashima, H.; Kase, K.; Domen, K. *Appl. Catal. A: Gen.* **2009**, *81*, 927–937.
(15) Hitoki, G.; Ishikawa, A.; Takata, T.; Kondo, J. N.; Hara, M.; Domen, K. *Chem. Lett.* **2002**, *31*, 736–737.
(16) Lee, Y.; Nukumizu, K.; Watanabe, T.; Takata, T.; Hara, M.; Yoshimura, M.; Domen, K. *Chem. Lett.* **2006**, *35*, 352–353.
(17) Kasahara, A.; Nukumizu, K.; Hitoki, G.; Takata, T.; Kondo, J. N.; Hara, M.; Kobayashi, H.; Domen, K. *J. Phys. Chem. A* **2002**, *106*, 6750–6753.
(18) Kasahara, A.; Nukumizu, K.; Takata, T.; Kondo, J. N.; Hara, M.; Kobayashi, H.; Domen, K. *J. Phys. Chem. B* **2003**, *107*, 791–797.
(19) (a) Abe, R.; Takata, T.; Sugihara, H.; Domen, K. *Chem. Commun.* **2005**, 3829–3831. (b) Higashi, M.; Abe, R.; Ishikawa, A.; Takata, T.; Ohtani, B.; Domen, K. *Chem. Lett.* **2008**, *37*, 138–139.
(20) (a) Higashi, M.; Abe, R.; Teramura, K.; Takata, T.; Ohtani, B.; Domen, K. *Chem. Phys. Lett.* **2008**, *452*, 120–123. (b) Higashi, M.; Abe, R.; Takata, T.; Domen, K. *Chem. Mater.* **2009**, *21*, 1543–1549.
(21) Sato, J.; Saito, N.; Yamada, Y.; Maeda, K.; Takata, T.; Kondo, J. N.; Hara, M.; Kobayashi, H.; Domen, K.; Inoue, Y. *J. Am. Chem. Soc.* **2005**, *127*, 4150–4151.
(22) Lee, Y.; Watanabe, T.; Takata, T.; Hara, M.; Yoshimura, M.; Domen, K. *J. Phys. Chem. B* **2006**, *110*, 17563–17569.
(23) Maeda, K.; Saito, N.; Lu, D.; Inoue, Y.; Domen, K. *J. Phys. Chem. C* **2007**, *111*, 4749–4755.
(24) Maeda, K.; Saito, N.; Inoue, Y.; Domen, K. *Chem. Mater.* **2007**, *19*, 4092–4097.
(25) Maeda, K.; Takata, T.; Hara, M.; Saito, N.; Inoue, Y.; Kobayashi, H.; Domen, K. *J. Am. Chem. Soc.* **2005**, *127*, 8286–8287.
(26) Maeda, K.; Teramura, K.; Takata, T.; Hara, M.; Saito, N.; Toda, K.; Inoue, Y.; Kobayashi, H.; Domen, K. *J. Phys. Chem. B* **2005**, *109*, 20504–20510.
(27) (a) Yashima, M.; Maeda, K.; Teramura, K.; Takata, T.; Domen, K *Chem. Phys. Lett.* **2005**, *416*, 225–227. (b) Yashima, M.; Maeda, K.; Teramura, K.; Takata, T.; Domen, K *Mater. Trans.* **2006**, *47*, 295–297.
(28) Teramura, K.; Maeda, K.; Saito, T.; Takata, T.; Saito, N.; Inoue, Y.; Domen, K. *J. Phys. Chem. B* **2005**, *109*, 21915–21921.
(29) Maeda, K.; Teramura, K.; Lu, D.; Takata, T.; Saito, N.; Inoue, Y.; Domen, K. *Nature* **2006**, *440*, 295.
(30) Maeda, K.; Teramura, K.; Saito, N.; Inoue, Y.; Domen, K. *J. Catal.* **2006**, *243*, 303–308.
(31) Maeda, K.; Teramura, K.; Lu, D.; Takata, T.; Saito, N.; Inoue, Y.; Domen, K. *J. Phys. Chem. B* **2006**, *110*, 13753–13758.

(32) Maeda, K.; Teramura, K.; Masuda, H.; Takata, T.; Saito, N.; Inoue, Y.; Domen, K. *J. Phys. Chem. B* **2006**, *110*, 13107–13112.
(33) Maeda, K.; Teramura, K.; Lu, D.; Saito, N.; Inoue, Y.; Domen, K. *Angew. Chem., Int. Ed.* **2006**, *45*, 7806–7809.
(34) Maeda, K.; Teramura, K.; Lu, D.; Saito, N.; Inoue, Y.; Domen, K. *J. Phys. Chem. C* **2007**, *111*, 7554–7560.
(35) Maeda, K.; Teramura, K.; Domen, K. *Catal. Surv. Asia* **2007**, *11*, 145–157.
(36) Maeda, K.; Lu, D.; Teramura, K.; Domen, K. *J. Mater. Chem.* **2008**, *18*, 3539–3542.
(37) Maeda, K.; Teramura, K.; Domen, K. *J. Catal.* **2008**, *254*, 198–204.
(38) Maeda, K.; Hashiguchi, H.; Masuda, H.; Abe, R.; Domen, K. *J. Phys. Chem. C* **2008**, *112*, 3447–3452.
(39) Sun, X.; Maeda, K.; Le Faucheur, M.; Teramura, K.; Domen, K. *Appl. Catal. A: Gen.* **2007**, *327*, 114–121.
(40) Hisatomi, H.; Maeda, K.; Lu, D.; Domen, K. *Chem Sus Chem* **2009**, *2*, 336–343.
(41) Lee, Y.; Terashima, H.; Shimodaira, Y.; Teramura, K.; Hara, M.; Kobayashi, H.; Domen, K.; Yashima, M. *J. Phys. Chem. C* **2007**, *111*, 1042–1048.
(42) Lee, Y.; Teramura, K.; Hara, M.; Domen, K. *Chem. Mater.* **2007**, *19*, 2120–2127.
(43) Wang, X.; Maeda, K.; Lee, Y.; Domen, K. *Chem. Phys. Lett.* **2008**, *457*, 134–136.
(44) Tessier, F.; Maillard, P.; Lee, Y.; Bleugat, C.; Domen, K. *J. Phys. Chem. C* **2009**, *113*, 8526–8531.
(45) Nakamura, S.; Mukai, T.; Senoh, M. *Appl. Phys. Lett.* **1994**, *64*, 1687–1689.
(46) Nakamura, S. *Science* **1998**, *281*, 956–961.
(47) Kocha, S. S.; Peterson, M. W.; Arent, D. J.; Redwing, J. M.; Tischler, M. A.; Turner, J. A. *J. Electrochem. Soc.* **1995**, *142*, L238–L240.
(48) Huygens, I. M.; Strubbe, K.; Gomes, W. P. *J. Electrochem. Soc.* **2000**, *147*, 1797–1802.
(49) Beach, J. D.; Collins, R. T.; Turner, J. A. *J. Electrochem. Soc.* **2003**, *150*, A899–A904.
(50) Wei, S. H.; Zunger, A. *Phys. Rev. B* **1988**, *37*, 8958–8981.
(51) Suhulz, H.; Thiemann, K. H. *Solid State Commun.* **1977**, *23*, 815–819.
(52) Garcia-Martinez, O.; Rojas, R. M.; Vila, E.; Martin de Vidales, J. L. *Solid State Ionics* **1997**, *63*, 442–449.
(53) Tessier, F.; Marchand, R. *J. Alloys Compd.* **1997**, *262*−*263*, 410–415.
(54) Tessier, F.; Marchand, R.; Laurent, Y. *J. Eur. Ceram. Soc.* **1997**, *17*, 1825–1829.
(55) Marchand, R.; Tessier, F.; DiSalvo, F. J. *J. Mater. Chem.* **1999**, *9*, 297–304.
(56) Schwenzer, B.; Loeffler, L.; Seshadri, R.; Keller, S.; Lange, F. F.; DenBaars, S. P.; Mishra, U. K. *J. Mater. Chem.* **2004**, *14*, 637–641.
(57) Hisatomi, T.; Teramura, K.; Kubota, J.; Domen, K. *Bull. Chem. Soc. Jpn.* **2008**, *81*, 1647–1656.
(58) Shannon, R. D. *Acta Crystallogr., Sect. A* **1976**, *32*, 751–767.
(59) Hirai, T.; Maeda, K.; Yoshida, M.; Kubota, J.; Ikeda, S.; Matsumura, M.; Domen, K. *J. Phys. Chem. C* **2007**, *111*, 18853–18855.
(60) (a) Jensen, L. L.; Muckerman, J. T.; Newton, M. D. *J. Phys. Chem. C* **2008**, *112*, 3439–3446. (b) Wei, W.; Dai, Y.; Yang, K.; Guo, M.; Huang, B. *J. Phys. Chem. C* **2008**, *112*, 15915–15919.
(61) Gerischer, H. *J. Electrochem. Soc.* **1966**, *113*, 1174–1182.
(62) Maeda, K.; Teramura, K.; Saito, N.; Inoue, Y.; Domen, K. *Bull. Chem. Soc. Jpn.* **2007**, *80*, 1004–1010.
(63) Lide, D. R. *Handbook of Chemistry and Physics*, 83rd ed.; CRC Press: Boca Raton, FL, 2002.
(64) Chen, H.; Wen, W.; Wang, Q.; Hanson, J. C.; Muckerman, J. T.; Fujita, E.; Frenkel, A. I.; Rodriguez, J. A. *J. Phys. Chem. C* **2009**, *113*, 3650–3659.
(65) Bechstedt, F.; Furthmuller, J. *J. Cryst. Growth* **2002**, *246*, 315–319.
(66) Kamata, K.; Maeda, K.; Lu, D.; Kako, Y.; Domen, K. *Chem. Phys. Lett.* **2009**, *470*, 90–94.